Extreme near-field heat transfer between gold surfaces

Takuro Tokunaga, Amun Jarzembski, Takuma Shiga, Keunhan Park, and Mathieu Francoeur

Phys. Rev. B **104**, 125404 — Published 2 September 2021

DOI: 10.1103/PhysRevB.104.125404

Extreme Near-Field Heat Transfer Between Gold Surfaces

Takuro Tokunaga,[1] Amun Jarzembski,[2] Takuma Shiga,[3] Keunhan Park,[1,*] and Mathieu Francoeur[1,†]

[1] *Department of Mechanical Engineering, University of Utah, Salt Lake City, Utah 84112, United States.*

[2] *Sandia National Laboratories, Albuquerque, NM 87185, United States.*

[3] *Department of Mechanical Engineering, The University of Tokyo, Bunkyo, Tokyo 113-8656, Japan.*

Extreme near-field heat transfer between metallic surfaces is a subject of debate as the state-of-the-art theory and experiments are in disagreement on the energy carriers driving heat transport. In an effort to elucidate the physics of extreme near-field heat transfer between metallic surfaces, this work presents a comprehensive model combining radiation, acoustic phonon and electron transport across sub-10-nm vacuum gaps. The results obtained for gold surfaces show that in the absence of bias voltage, acoustic phonon transport is dominant for vacuum gaps smaller than ∼2 nm. The application of a bias voltage significantly affects the dominant energy carriers as it increases the phonon contribution mediated by the long-range Coulomb force and the electron contribution due to a reduced potential barrier. For a bias voltage of 0.6 V, acoustic phonon transport becomes dominant at a vacuum gap of 5 nm, whereas electron tunneling dominates at sub-nm vacuum gaps. The comparison of the theory against experimental data from the literature suggests that well-controlled measurements between metallic surfaces are needed to quantify the

contributions of acoustic phonon and electron as a function of the bias voltage.

I. INTRODUCTION

Radiative heat transfer between two surfaces separated by a sub-wavelength vacuum gap can exceed the far-field blackbody limit by a few orders of magnitude owing to tunneling of evanescent electromagnetic waves [1]. Theoretical predictions of near-field radiative heat transfer based on fluctuational electrodynamics [2] are well-established, and have been experimentally validated in various configurations for nanosized vacuum gaps [3–18]. However, fluctuational electrodynamics may not be able to accurately describe heat transfer in the extreme near-field regime, defined here as sub-10-nm vacuum gap distances, due to its macroscopic nature involving local field averaging (i.e., local dielectric function) [19]. In addition, fluctuational electrodynamics solely accounts for electromagnetic waves (i.e., radiation), whereas acoustic phonons and electrons may also contribute to heat transport between surfaces separated by single-digit nanometer vacuum gaps prior to contact. A few theoretical works have investigated acoustic phonon transport across vacuum gaps [19–30], and some have explicitly shown the inadequacy of fluctuational electrodynamics for modeling heat transfer in the extreme near field [19, 21, 23–30].

Experimental measurements of extreme near-field heat transfer are scarce [31–36]. Jarzembski *et al.* [36] measured a thermal conductance exceeding fluctuational electrodynamics predictions by three orders of magnitude between a silicon tip and a platinum nanoheater separated by sub-10-nm vacuum gaps down to contact. By considering all energy carriers, it was shown quantitatively that heat transfer across nanometer-sized vacuum gaps can be dominated by acoustic phonon transport mediated by van der Waals and Coulomb forces. Extreme near-field heat transfer between metallic surfaces has also been measured,

but drastically different results have been reported. Kim *et al.* [33] measured heat transfer between a thermocouple-embedded tip fabricated at the free-end of a stiff cantilever and a suspended resistive microheater at 305 K. Their measurements between a gold (Au)-coated tip and an Au surface are in good agreement with fluctuational electrodynamics down to a vacuum gap of ∼2 nm. On the other hand, Kloppstech *et al.* [34] reported the measurement of heat transfer between an Au thermocouple-embedded scanning tunneling microscope tip and a cryogenically-cooled Au surface, observing heat transfer largely exceeding fluctuational electrodynamics for vacuum gaps from 7 nm down to 0.2 nm. However, no comprehensive modeling was performed to quantitatively support their observation. Subsequently, Cui *et al.* [35] measured heat transfer between an Au-coated tip and an Au surface, both subjected to various surface-cleaning procedures, for vacuum gaps from 5 nm down to a few Å. They hypothesized that the large heat transfer reported by Kloppstech *et al.* [34] may be due to a low apparent potential barrier for electron tunneling mediated by surface contaminants bridging the tip and the surface prior to bulk contact.

A few theoretical works have analyzed extreme near-field heat transfer between Au surfaces [23, 25–30]. Using a surface perturbation approach, Pendry *et al.* [23] predicted that the heat transfer coefficient due to acoustic phonons exceeds that obtained with fluctuational electrodynamics for vacuum gaps smaller than 0.4 nm. Similar results were obtained by Volokitin [28]. Alkurdi *et al.* [27] compared the contributions of radiation, phonons and electrons to heat transfer between Au surfaces separated by vacuum gaps varying from 1.5 nm down to 0.2 nm. Using a three-dimensional (3D) lattice dynamics framework, it was found that acoustic phonon transport exceeds radiation for all vacuum gaps considered, whereas electron tunneling slightly surpasses the phonon contribution for vacuum gaps smaller than 0.4 nm. In stark contrast, Messina *et al.* [26] predicted that acoustic phonon transport does

not play any role in extreme near-field heat transfer between Au surfaces. Their results indicated that for vacuum gaps smaller than ∼1 nm, electron tunneling largely dominates heat transfer, whether or not a bias voltage is applied between the two surfaces. Volokitin showed that surface charges induced by a bias voltage [28, 29] and the electrical double layer effect [30] between Au surfaces increase the contribution of TM-polarized electromagnetic waves in the extreme near field.

Despite these experimental and theoretical efforts, the mechanisms driving heat transfer between metallic surfaces separated by sub-10-nm vacuum gaps are not well understood. The objective of this work is to elucidate the physics underlying extreme near-field heat transfer between Au surfaces, and to determine vacuum gap ranges in which radiation, phonon, and electron are the dominant carriers. This is achieved by implementing a comprehensive model that accounts for all energy carriers, and by comparing theoretical predictions against the experimental data from Refs. [26, 33, 34]. It is shown that in the absence of bias voltage, heat transfer is mediated by acoustic phonon transport for vacuum gaps smaller than ∼2 nm. In addition, applying a bias voltage between Au surfaces enhances the contributions of acoustic phonon and electron tunneling owing to the long-range Coulomb force and the lower potential barrier, respectively.

II. DESCRIPTION OF THE MODEL

To compare the theory against experimental results, the thermal conductance G between a tip and a surface separated by a vacuum gap d is calculated from local heat transfer coefficients h between two parallel surfaces, modeled as semi-infinite layers, using the Derjaguin

approximation [3, 37]:

$$G = \int_0^{r_{\rm tip}} dr h(\tilde{d}) 2\pi r \tag{1}$$

where r is the radial direction, $r_{\rm tip}$ is the tip radius, and $\tilde{d} = d + r_{\rm tip} - \sqrt{{r_{\rm tip}}^2 - r^2}$ is the vacuum gap distance between the surfaces: see Fig. 1. The heat transfer coefficient in Eq. (1) is the sum of contributions from radiation, phonon, and electron, as detailed hereafter.

A. Radiation transport

The heat transfer coefficient due to radiation between two parallel surfaces (media L and R) separated by a vacuum gap of thickness $\tilde{d}$ (medium 0) is calculated using fluctuational electrodynamics to account for the near-field effects [1]:

$$h_{\rm rad} = \frac{1}{\pi^2 (T_{\rm L} - T_{\rm R})} \int_0^\infty d\omega \left[\Theta\left(\omega, T_{\rm L}\right) - \Theta\left(\omega, T_{\rm R}\right)\right] \int_0^\infty dk_\rho k_\rho \sum_{\gamma={\rm TE,TM}} \mathcal{T}^\gamma_{\rm rad}\left(\omega, k_\rho\right) \tag{2}$$

where ω is the angular frequency, k_ρ is the component of the wavevector parallel to an interface, and $\Theta(\omega, T)$ is the mean energy of an electromagnetic state calculated as $\hbar\omega/[\exp(\hbar\omega/k_{\rm b}T) - 1]$. The transmission functions in polarization state γ for propagating ($k_\rho < k_0$) and evanescent ($k_\rho > k_0$) electromagnetic waves in vacuum are respectively given by:

$$\mathcal{T}^\gamma_{\rm rad,prop}\left(\omega, k_\rho\right) = \frac{\left(1 - |r^\gamma_{\rm 0L}|^2\right)\left(1 - |r^\gamma_{\rm 0R}|^2\right)}{4\left|1 - r^\gamma_{\rm 0L} r^\gamma_{\rm 0R} e^{2i{\rm Re}(k_{\rm z0})\tilde{d}}\right|^2} \tag{3}$$

$$\mathcal{T}^\gamma_{\rm rad,evan}\left(\omega, k_\rho\right) = e^{-2{\rm Im}(k_{\rm z0})\tilde{d}} \frac{{\rm Im}\left(r^\gamma_{\rm 0L}\right){\rm Im}\left(r^\gamma_{\rm 0R}\right)}{\left|1 - r^\gamma_{\rm 0L} r^\gamma_{\rm 0R} e^{-2{\rm Im}(k_{\rm z0})\tilde{d}}\right|^2} \tag{4}$$

where $k_{\rm z0}$ is the component of the vacuum wavevector perpendicular to an interface, and r^γ_{0j} ($j = {\rm L, R}$) is the Fresnel reflection coefficient [38]. The frequency-dependent dielectric function of Au is calculated using the Drude model provided in Ref. [39].

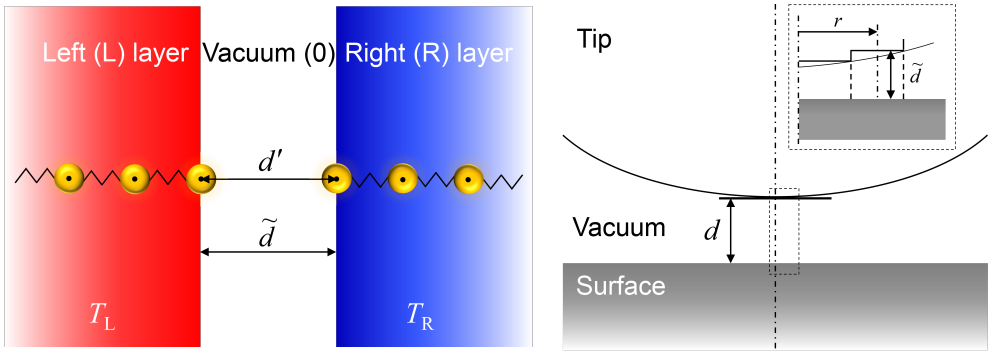

FIG. 1: The thermal conductance between a tip and a surface separated by a vacuum gap d is calculated from the heat transfer coefficients between two parallel surfaces, modeled as semi-infinite layers, separated by a vacuum gap $\tilde{d}$ using the Derjaguin approximation. Top-most atoms are located at the Au-vacuum interfaces. The interatomic vacuum distance d' used for predicting acoustic phonon transport is the same as the vacuum gap thickness $\tilde{d}$ used for radiation and electron tunneling calculations. The left (L) and right (R) semi-infinite layers are assumed to be at constant and uniform temperatures $T_{\rm L}$ and $T_{\rm R}$.

B. Acoustic phonon transport

Acoustic phonons can tunnel across vacuum gaps via force interactions. Acoustic phonon transport is modeled using the one-dimensional (1D) atomistic Green's function (AGF) method [40, 41]. The heat transfer coefficient due to acoustic phonon transport across an interatomic vacuum distance d' for a 1D atomic chain is written as:

$$h_{\mathrm{ph}} = \frac{1}{A(T_{\mathrm{L}} - T_{\mathrm{R}})} \int_0^\infty d\omega \frac{\hbar\omega}{2\pi} \mathcal{T}_{\mathrm{ph}}(\omega)[N(\omega, T_{\mathrm{L}}) - N(\omega, T_{\mathrm{R}})] \tag{5}$$

where $N = 1/[\exp(\hbar\omega/k_{\mathrm{b}}T) - 1]$ is the Bose-Einstein distribution function and A is the cross-sectional area of an atom. The atomic radius of Au is taken as 1.740 Å [42]. The top-most atoms are located at the Au-vacuum interfaces [43], such that the interatomic vacuum distance d' is the same as the vacuum gap thickness $\tilde{d}$ used for radiation and electron transport calculations (see Fig. 1). Note that the lattice constant of Au (4.065 Å) is used as the criterion for bulk contact. The minimum distance at which the heat transfer coefficient is calculated is therefore 4.065 Å. The phonon transmission function is given by the Caroli formula [44]:

$$\mathcal{T}_{\mathrm{ph}}(\omega) = \mathrm{Trace}[\Gamma_{\mathrm{L}} G_{\mathrm{d}} \Gamma_{\mathrm{R}} G_{\mathrm{d}}^{\dagger}] \tag{6}$$

where the superscript † denotes conjugate transpose, $\Gamma_{\mathrm{L,R}}$ is the escape rate of phonons from the device region to the semi-infinite layers, and G_{d} is the Green's function of the device region. In the present study, the device region encompasses the vacuum gap and five atoms in each of the semi-infinite layers. Increasing the number of atoms in the device region does not affect the phonon transmission function. Details about the 1D AGF method have been provided in Refs. [36, 40, 41].

Short- and long-range force interactions are considered for modeling acoustic phonon transport across vacuum gaps. For the short-range interactions, the Lennard-Jones model

is used to account for the van der Waals force and overlapping electron cloud repulsive force [45–47]. The Lennard-Jones model is provided in Sec. S1 of the Supplemental Material [48]. When there is a bias voltage, the induced surface charges generate long-range capacitance and Coulomb forces [49–52]. The capacitance force between Au atoms is derived from the capacitance force between a tip and a surface [48]:

$$F_{\text{Capacitance}} = \frac{\epsilon_0 V_{\text{bias}}^2}{2} \frac{A}{d'^2} \tag{7}$$

where ϵ_0 is the permittivity of free space and V_{bias} is the bias voltage. Similarly, the Coulomb force between Au atoms is calculated from the Coulomb force due to surface charges between a tip and a surface [48]:

$$F_{\text{Coulomb}} = \frac{Q_{\text{s}} Q_{\text{t}}}{4\pi\epsilon_0 d'^2} \frac{A}{A_{\text{tip}}} \tag{8}$$

where A_{tip} is the tip surface, Q_{s} is the surface charge, and Q_{t} is the tip charge defined as $Q_{\text{t}} = -(Q_{\text{s}} + Q_{\text{e}})$. The induced capacitive charge is given by $Q_{\text{e}} = CV_{\text{bias}}$, where C $(= \epsilon_0 A_{\text{tip}}/d)$ is the parallel plate capacitance [53]. At the onset of contact, the Coulomb force vanishes due to charge neutralization [54]. The reduction of the surface charge density $(Q_{\text{s}}/A_{\text{tip}})$ with respect to the vacuum gap separating a tip and a surface has been previously predicted [55, 56]. In addition, an experimental effort has demonstrated a vanishing capacitance between a tip and a substrate with the reduction of the vacuum gap distance [57]. As such, the surface charge density should ideally be treated as a function of the interatomic distance [56]. However, since it is challenging to develop a distance-dependent surface charge density model, $Q_{\text{s}}/A_{\text{tip}}$ is treated here as a constant value, which is a reasonable assumption for gap distances of a few nanometers [55], that vanishes below a cut-off vacuum distance [58]. The cut-off value is approximated as the interatomic vacuum distance for which electron tunneling becomes significant, corresponding to $d' \approx 7\,\text{Å}$ [59]. Jarzembski *et al.* [36] estimated the surface

charge density of a biased platinum surface based on their experimental conditions. A surface charge density of 8×10^{-4} C/m^2 was estimated for a bias voltage of 0.8 V. In the present work, a value of 6×10^{-4} C/m^2 is used for $V_{\text{bias}} = 0.6$ V under the assumption that the surface charge density varies linearly with the bias voltage [60, 61].

The validity of the capacitance and Coulomb force models at nanosized vacuum gaps is justified as follows. The capacitance force model based on Eq. (7) has been validated down to a vacuum gap of ∼10 nm via force microscopy between a nickel probe and a PMMA surface [62] and down to ∼5 nm via atomic force microscopy (AFM) between a tungsten tip and a silicon surface [63]. In addition, El Khoury *et al.* [64] measured force gradients between an AFM probe and epoxy surfaces, and found an excellent agreement between experiments and theory based on the capacitance and Coulomb force models given by Eqs. (7) and (8) down to a vacuum gap of 10 nm.

For the vacuum gap distances considered in this work, the Coulomb force largely exceeds the capacitance force (see Fig. S1 of Sec. 2 of the Supplemental Material [48]). Therefore, the total force driving acoustic phonon transport across vacuum gaps between two Au surfaces is given as the sum of the Lennard-Jones force model ($F_{\text{L-J}}$) and the Coulomb force (F_{Coulomb}):

$$F_{\text{total}} = F_{\text{L-J}} + F_{\text{Coulomb}} \tag{9}$$

The inputs for AGF calculations are the force constants, which are obtained by taking the absolute values of the first order derivative of F_{total} with respect to d' (i.e., $\left|\partial F_{\text{total}}/\partial d'\right|$) [21].

C. Electron transport

Electrons can contribute to heat transfer across vacuum gaps via tunneling and thermionic emission. Owing to the low temperatures considered (∼300 K), thermionic emission is negligible. The heat transfer coefficient due to electron tunneling across a vacuum gap can be written as [65–67]:

$$h_{\mathrm{el}} = \frac{1}{(T_{\mathrm{L}}-T_{\mathrm{R}})}\int_{-\infty}^{W_{\max}} dE_z[\,(E_z+k_{\mathrm{b}}T_{\mathrm{L}})\,N_{\mathrm{L}}\,(E_z,T_{\mathrm{L}}) - (E_z+k_{\mathrm{b}}T_{\mathrm{R}})\,N_{\mathrm{R}}\,(E_z-eV_{\mathrm{bias}},T_{\mathrm{R}})]\mathcal{T}_{\mathrm{el}}\,(E_z) \tag{10}$$

where $e = 1.602\times10^{-19}\,\mathrm{C}$ is the electron charge, E_z is the electron energy perpendicular to the surfaces, and $W_{\max}$ is the maximum potential barrier. The term $N_j(E_z,T_j)$, denoting the number of electrons at energy level E_z per unit area and per unit time, is calculated as [65]:

$$N_j\,(E_z,T_j) = \frac{m_{\mathrm{e}}k_{\mathrm{b}}T_j}{2\pi^2\hbar^3}\ln\left[1+\exp\left(-\frac{E_z-E_{F,j}}{k_{\mathrm{b}}T_j}\right)\right] \tag{11}$$

where $m_{\mathrm{e}} = 9.109\times10^{-31}\,\mathrm{kg}$ is the electron mass, and $E_{F,j}$ is the Fermi level used as a reference for computing the electron energy [65]. The electron transmission function is calculated using the Wentzel-Kramers-Brillouin (WKB) approximation [68]:

$$\mathcal{T}_{\mathrm{el}}\,(E_z) = \exp\left[-\frac{\sqrt{8m_{\mathrm{e}}}}{\hbar}\int_{z_1}^{z_2} dz\sqrt{W\,(z)-E_z}\right] \tag{12}$$

where $W(z)$ is the potential barrier profile in the vacuum gap, while z_1 and z_2 are the roots of $W(z)-E_z=0$ delimiting the width of the electron tunneling barrier E_z. The potential barrier profile can be expressed as [65]:

$$W(z) = W_{id}(z) + W_{ic}(z) \tag{13}$$

Note that the space-charge effect is assumed to be fully suppressed for sub-10-nm vacuum gaps [67]. The ideal barrier profile [67] and image-charge perturbation [69] are respectively

calculated as:

$$W_{id}(z) = \Phi_{\mathrm{L}} - (\Phi_{\mathrm{L}} - \Phi_{\mathrm{R}} - eV_{\mathrm{bias}}) \left(\frac{z}{\tilde{d}}\right) \tag{14}$$

$$W_{ic}(z) = \frac{e^2}{16\pi\epsilon_0 d}\left[-2\Psi\left(1\right) + \Psi\left(\frac{z}{\tilde{d}}\right) + \Psi\left(1 - \frac{z}{\tilde{d}}\right)\right] \tag{15}$$

where $\Phi_{\mathrm{L,R}} = 5.10$ eV is the work function of Au [70] and Ψ is the digamma function.

The WKB approximation may lead to an overestimation of the electron heat transfer coefficient below vacuum gaps of ∼0.5 nm [66, 71]. As such, for small vacuum gaps, the electron heat transfer coefficient is also calculated via the 1D non-equilibrium Green's function (NEGF) approach described in Ref. [66]. In the NEGF framework, the electron transmission function is given by:

$$\mathcal{T}_{\mathrm{el}}(E_z) \;=\; \mathrm{Trace}[\Gamma_{\mathrm{L}} G^{\mathrm{R}} \Gamma_{\mathrm{R}} \left(G^{\mathrm{R}}\right)^{\dagger}], \tag{16}$$

where $\Gamma_{\mathrm{L,R}}$ is the energy broadening matrix, whereas G^{R} is the retarded Green's function.

III. RESULTS

The heat transfer coefficients between two Au surfaces due to radiation, acoustic phonon transport, and electron tunneling are presented in Fig. 2(a) for the experimental conditions taken from Kim *et al.* [33], where $T_{\mathrm{L}} = 305$ K, $T_{\mathrm{R}} = 300$ K, and $V_{\mathrm{bias}} = 0$ V. The Au-vacuum interfaces support surface plasmon polaritons at a high frequency ($\sim 1.2 \times 10^{16}$ rad/s) that cannot be thermally excited at room temperature. As such, the radiation heat transfer coefficient, dominated by TE-polarized electromagnetic waves, saturates as the vacuum gap decreases. It should be noted that while fluctuational electrodynamics is not expected to be valid for sub-2-nm vacuum gaps owing to non-local effects [39], radiation predictions below 2 nm vacuum gaps are shown throughout the paper for reference. In addition, the

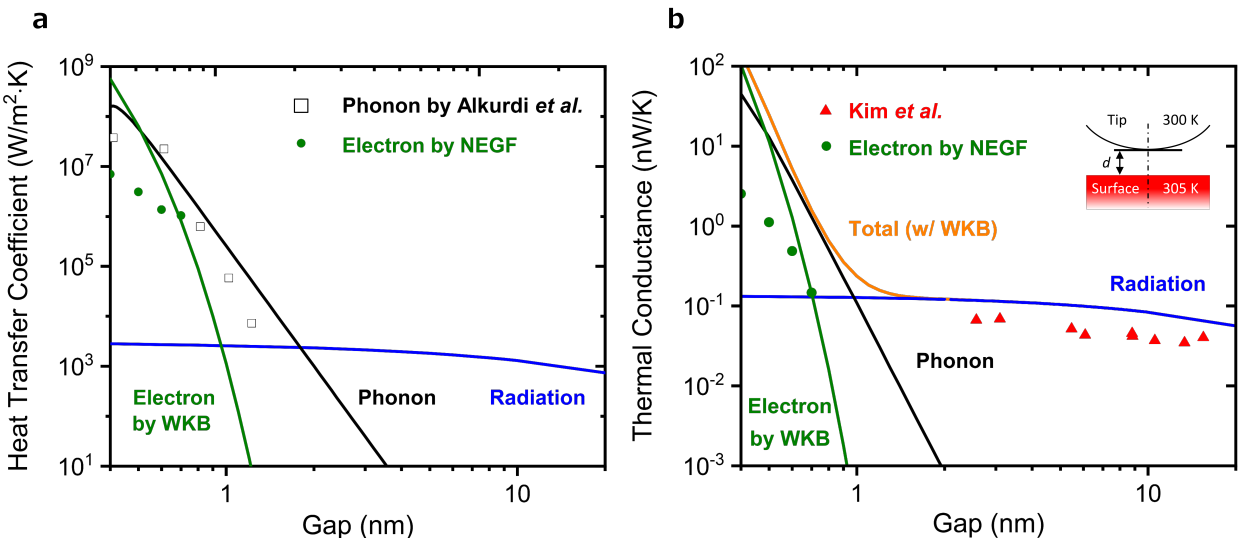

FIG. 2: (a) Heat transfer coefficients due to radiation, phonon, and electron between two Au surfaces separated by a vacuum gap $\tilde{d}$ ($T_{\mathrm{L}} = 305$ K, $T_{\mathrm{R}} = 300$ K, $V_{\mathrm{bias}} = 0$ V). The electron heat transfer coefficient is calculated via the WKB approximation and the NEGF. The phonon heat transfer coefficient predicted via the 1D AGF method is compared against the 3D lattice dynamics results of Alkurdi *et al.* [27]. (b) Thermal conductance between a 450-nm-radius tip (300 K) and a surface (305 K), both made of Au, separated by a vacuum gap d. The total conductance is calculated using the electron heat transfer coefficient from the WKB approximation. The predicted conductance is compared against the experimental results of Kim *et al.* [33].

enhancement of TM-polarized electromagnetic waves mediated by the electrical double layer effect (no bias voltage) [30] and by surface charges induced by a bias voltage [28, 29] is not taken into account in the radiation model. As explained hereafter, these effects have no impact on the calculated thermal conductance.

In the absence of bias voltage, only the van der Waals and overlapping electron cloud forces, represented by the Lennard-Jones model, contribute to acoustic phonon transport. The phonon heat transfer coefficient exceeds that of radiation for a vacuum gap smaller than ∼2 nm. This result contrasts with the results of Refs. [23, 28] where acoustic phonon transport exceeds radiation transfer for vacuum gaps smaller than ∼0.4 nm. This discrepancy can be explained by the different descriptions of the force interactions and phonon transmission in Refs. [23, 28]. It is worth noting that the accuracy of the 1D AGF approach used in this work is verified in Fig. 2(a) by comparison against the results obtained from a 3D lattice dynamics framework [27]. The electron heat transfer coefficient exceeds the radiation heat transfer coefficient for a vacuum gap smaller than ∼1 nm. Provided that the NEGF calculates the electron transmission function more accurately than the WKB approximation for vacuum gaps smaller than ∼0.5 nm [66, 71], the results indicate that the phonon contribution always exceed that of the electron for sub-2-nm vacuum gaps near room temperature.

Figure 2(b) shows the predicted thermal conductance between a 450-nm-radius Au tip at 300 K and an Au surface at 305 K by applying the Derjaguin approximation with the heat transfer coefficients shown in Fig. 2(a). These predictions are compared against the conductance measured in Ref. [33] for vacuum gaps down to ∼2 nm. Clearly, for vacuum gaps larger than ∼1.5 nm, heat transfer is mediated by radiation. The calculated total conductance is in good agreement with the experimental data of Ref. [33]. The results

from the comprehensive model presented in this work therefore support the conclusions of Kim *et al.* [33]. Vacuum gaps approximately equal to or smaller than 1 nm would have been required to observe a significant enhancement of the conductance mediated by acoustic phonon transport. Note that including the electrical double layer effect [30] in the radiation transport model does not impact the thermal conductance in the vacuum gap range considered in Kim *et al.* [33]: see Sec. 3 of the Supplemental Material [48].

Figure 3(a) presents the heat transfer coefficients between two Au surfaces due to radiation, acoustic phonon transport, and electron tunneling for the experimental conditions taken from Kloppstech *et al.* [34], where $T_{\mathrm{L}} = 280$ K, $T_{\mathrm{R}} = 120$ K, and $V_{\mathrm{bias}} = 0.6$ V. The phonon heat transfer coefficient is calculated with and without bias voltage, and the shaded area in Fig. 3(a) shows its possible values. Owing to the long-range Coulomb force mediated by the bias voltage, the phonon heat transfer coefficient exceeds that of radiation for vacuum gaps smaller than ∼5 nm. The Coulomb force, however, has a low impact on the phonon heat transfer coefficient for vacuum gaps smaller than 1 nm. Note that these predictions are significantly larger than the acoustic phonon transport results under the electrostatic force for $V_{\mathrm{bias}} = 1$ V reported in Refs. [23, 28]. This is explained by the fact that Refs. [23, 28] only take into account the capacitance force, which is significantly smaller than the Coulomb force. The electron heat transfer coefficient is enhanced due to the bias voltage that lowers the potential barrier for tunneling. The WKB approximation suggests that electron-mediated heat transfer exceeds acoustic phonon transport for vacuum gaps smaller than 1 nm. The NEGF also suggests that the electron heat transfer coefficient is slightly larger than that of phonon, but for sub-0.5-nm vacuum gaps.

The thermal conductance calculated between a 30-nm-radius Au tip and an Au surface is shown in Fig. 3(b) under the same experimental conditions as in Fig. 3(a) (temperatures

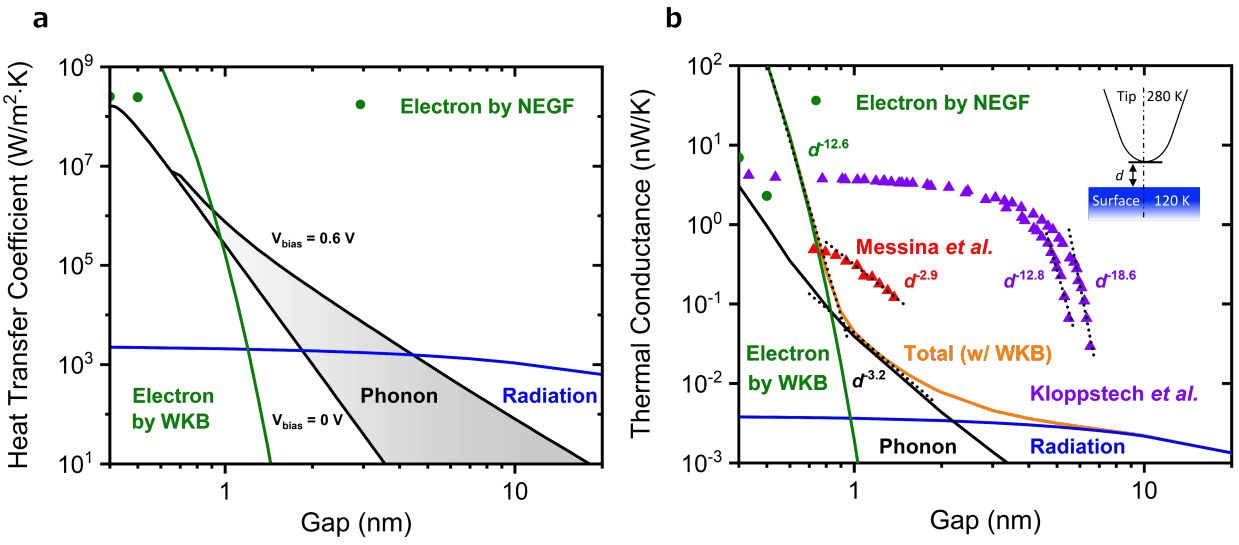

FIG. 3: (a) Heat transfer coefficients due to radiation, phonon, and electron between two Au surfaces separated by a vacuum gap $\tilde{d}$ ($T_{\mathrm{L}} = 280$ K, $T_{\mathrm{R}} = 120$ K, $V_{\mathrm{bias}} = 0.6$ V). The electron heat transfer coefficient is calculated via the WKB approximation and the NEGF. The phonon heat transfer coefficient is calculated both with and without bias voltage. (b) Thermal conductance between a 30-nm-radius tip (280 K) and a surface (120 K), both made of Au, separated by a vacuum gap d. The total conductance is calculated using the electron heat transfer coefficient from the WKB approximation. The predicted conductance is compared against the experimental results of Kloppstech *et al.* [34] and Messina *et al.* [26].

of 280 and 120 K, $V_{\text{bias}} = 0.6$ V). The results are compared against the experimental data of Kloppstech *et al.* [34], in addition to a more recent set of data from the same group [26]. Note that the most recent experimental data were obtained for surface and tip temperatures of respectively 195 K and 295 K. These slight temperature differences have no noticeable impact on the heat transfer coefficients: see Sec. S4 of the Supplemental Material [48]. The total conductance, which include the radiation, phonon, and electron contributions, display three distinct regimes. For vacuum gaps larger than 5 nm, radiation transport via evanescent electromagnetic waves drives heat transfer. For vacuum gaps from 5 nm down to ∼1.5 nm, radiation transitions to acoustic phonon-mediated heat transfer. Acoustic phonon transport becomes dominant between vacuum gaps of 1.5 nm and 0.9 nm. For vacuum gaps smaller than 0.9 nm, electron tunneling drives heat transfer owing to the applied bias voltage.

The magnitude of the experimental and theoretical data are quite different. Nevertheless, a power law analysis may enable determining the energy carriers driving heat transport in the experiments of Refs. [26, 34]. In the vacuum gap range of 1 nm to 1.5 nm where acoustic phonon transport is dominant, the predicted total conductance follows a $d^{-3.2}$ power law. Within that range, the data of Messina *et al.* [26] vary as $d^{-2.9}$, which is close to the theory. This regime arises due to the Coulomb force induced by the bias voltage. For vacuum gaps smaller than 0.9 nm where electron tunneling dominates heat transport, the total conductance follows a $d^{-12.6}$ power law. Interestingly, a similar trend is observed in the experimental data of Kloppstech *et al.* [34] but at much larger vacuum gaps ($d \gtrsim 5$ nm). It is worth noting that the enhancement of radiation transfer in TM polarization mediated by surface charges induced by a bias voltage, discussed in Refs. [28, 29], has no impact on the thermal conductance shown in Fig. 3(b). Indeed, for $V_{\text{bias}} = 1$ V, the TM component of the radiation heat transfer coefficient exceeds the TE contribution for vacuum gaps smaller

than ∼0.18 nm [28, 29]. Additionally, the radiation heat transfer coefficient that includes the electrical double layer effect [30] never exceeds the phonon heat transfer coefficient for $V_{\text{bias}} = 0.6$ V reported in Fig. 3(a). As such, the electrical double layer effect has no impact on the thermal conductance shown in Fig. 3(b).

It has been hypothesized that contaminants bridging the tip and the surface prior to bulk contact may lower the potential barrier for electron tunneling [35]. Using their measured tunneling current, Messina *et al.* [26] estimated an apparent potential barrier of 1 eV, which induces an enhancement of the electron heat transfer coefficient. Fig. 4 shows the thermal conductance predicted by considering a simple potential barrier of 1 eV for electron tunneling. As expected, electron tunneling for that case becomes dominant at a larger vacuum gap (∼1.5 nm). The magnitude of the total conductance is closer to the experimental data of Messina *et al.* [26], but the trends are different. Electron-mediated heat transport follows a $d^{-10.2}$ power law, which is not experimentally observed. In the gap range between 1.5 nm and 2 nm where all energy carriers contribute to the conductance, a $d^{-2.7}$ power law is predicted. This is again close to the $d^{-2.9}$ power law of Messina *et al.* [26] which however arises in a slightly different vacuum gap range (1 nm to 1.5 nm). It is concluded that the measured conductance reported by Messina *et al.* [26] is not solely due to electron tunneling. Rather, heat transport for this case is likely to be a combination of acoustic phonon transport, enhanced via the bias voltage, and electron tunneling possibly enhanced by the low apparent potential barrier mediated by contaminants. It has been pointed out that the data of Kloppstech *et al.* [34] were obtained at different apparent potential barrier heights [26], which make their interpretation challenging. Yet, the variation of the conductance with respect to the vacuum gap suggests electron-mediated heat transfer.

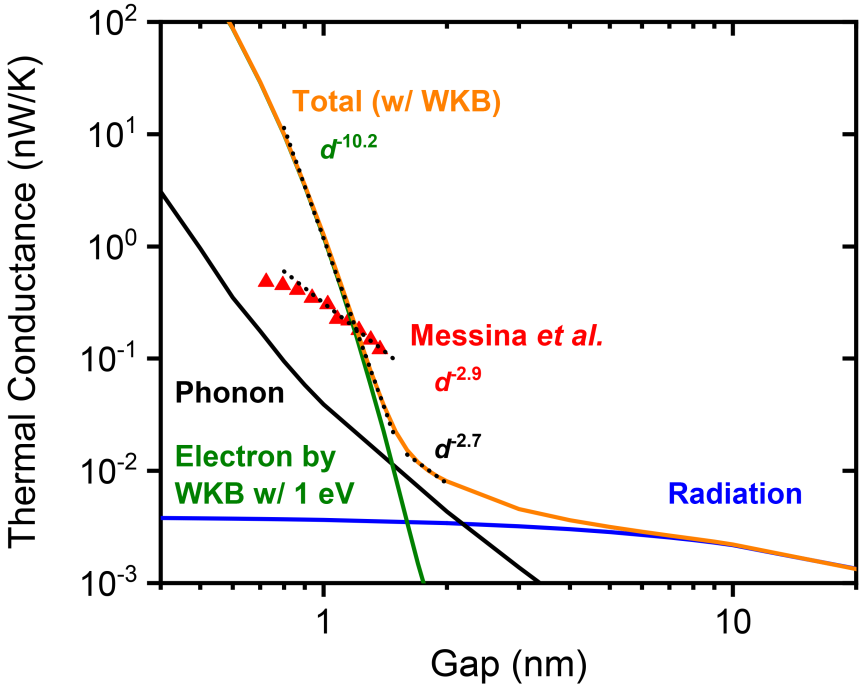

FIG. 4: Thermal conductance between a 30-nm-radius tip (280 K) and a surface (120 K), both made of Au, separated by a vacuum gap d. The electron heat transfer coefficient is calculated with the WKB approximation using an apparent potential barrier of 1 eV. The phonon heat transfer coefficient is calculated with a bias voltage of 0.6 V. The predicted conductance is compared against the experimental results of Messina *et al.* [26].

IV. CONCLUSIONS

In summary, a comprehensive model combining fluctuational electrodynamics for radiation, the AGF method for phonon, and the WKB approximation in addition to the NEGF approach for electron has been implemented to analyze extreme near-field heat transfer between Au surfaces. In the absence of bias voltage and near room temperature, heat transfer is mediated by radiation through evanescent electromagnetic waves down to a vacuum gap of ∼2 nm, below which acoustic phonon transport is the dominant energy carrier. It was shown that the application of a bias voltage increases not only electron tunneling, but also acoustic phonon transport mediated by the long-range Coulomb force. As a result, for a bias voltage of 0.6 V, acoustic phonon transport can affect heat transfer for vacuum gaps from 5 nm down to ∼1 nm, and electron tunneling should be a responsible heat transfer mechanism below 1 nm. However, comparison of the comprehensive model against state-of-the-art measurements [26, 33, 34] reveals that additional data are needed to experimentally quantify the contributions of acoustic phonons and electrons as a function of the bias voltage in the heat transfer between Au surfaces separated by sub-10-nm vacuum gaps.

ACKNOWLEDGMENTS

This work was supported by the National Science Foundation (grants CBET-1605584 and CBET-1952210). T.T. also appreciate the financial support by the Yamada Science Foundation and the Fujikura Foundation.

* Electronic address: kpark@mech.utah.edu

† Electronic address: mfrancoeur@mech.utah.edu

[1] D. Polder and M. Van Hove, Phys. Rev. B **4**, 3303 (1971).

[2] S. M. Rytov, Y. A. Kravtsov, and V. I. Tatarskii, *Principles of Statistical Radiophysics. 3 Elements of Random Fields* (Springer, New York, 1989).

[3] E. Rousseau, A. Siria, G. Jourdan, S. Volz, F. Comin, J. Chevrier, and J. J. Greffet, Nat. Photonics **3**, 514 (2009).

[4] S. Shen, A. Narayanaswamy, and G. Chen, Nano Lett. **9**, 2909 (2009).

[5] B. Song, Y. Ganjeh, S. Sadat, D. Thompson, A. Fiorino, V. Fernández-Hurtado, J. Feist, F. J. Garcia-Vidal, J. C. Cuevas, P. Reddy, et al., Nat. Nanotechnol. **10**, 253 (2015).

[6] B. Song, D. Thompson, A. Fiorino, Y. Ganjeh, P. Reddy, and E. Meyhofer, Nat. Nanotechnol. **11**, 509 (2016).

[7] R. St-Gelais, L. Zhu, S. Fan, and M. Lipson, Nat. Nanotechnol. **11**, 515 (2016).

[8] M. P. Bernardi, D. Milovich, and M. Francoeur, Nat. Commun. **7**, 12900 (2016).

[9] J. I. Watjen, B. Zhao, and Z. M. Zhang, Appl. Phys. Lett. **109**, 203112 (2016).

[10] K. Ito, K. Nishikawa, A. Miura, H. Toshiyoshi, and H. Iizuka, Nano Lett. **17**, 4347 (2017).

[11] A. Fiorino, D. Thompson, L. Zhu, B. Song, P. Reddy, and E. Meyhofer, Nano Lett. **18**, 3711 (2018).

[12] M. Lim, J. Song, S. S. Lee, and B. J. Lee, Nat. Commun. **9**, 4302 (2018).

[13] M. Ghashami, H. Geng, T. Kim, N. Iacopino, S. K. Cho, and K. Park, Phys. Rev. Lett. **120**, 175901 (2018).

[14] J. DeSutter, L. Tang, and M. Francoeur, Nat. Nanotechnol. **14**, 751 (2019).

[15] K. Shi, Y. Sun, Z. Chen, N. He, F. Bao, J. Evans, and S. He, Nano Lett. **19**, 8082 (2019).

[16] L. Tang, J. DeSutter, and M. Francoeur, ACS Photonics **7**, 1304 (2020).

[17] X. Ying, P. Sabbaghi, N. Sluder, and L. Wang, ACS Photonics **7**, 190 (2020).

[18] H. Salihoglu, W. Nam, L. Traverso, M. Segovia, P. K. Venuthurumilli, W. Liu, Y. Wei, W. Li, and X. Xu, Nano Lett. **20**, 6091 (2020).

[19] V. Chiloyan, J. Garg, K. Esfarjani, and G. Chen, Nat. Commun. **6**, 6755 (2015).

[20] M. Prunnila and J. Meltaus, Phys. Rev. Lett. **105**, 125501 (2010).

[21] Y. Ezzahri and K. Joulain, Phys. Rev. B **90**, 115433 (2014).

[22] S. Xiong, K. Yang, Y. A. Kosevich, Y. Chalopin, R. D'Agosta, P. Cortona, and S. Volz, Phys. Rev. Lett. **112**, 114301 (2014).

[23] J. B. Pendry, K. Sasihithlu, and R. V. Craster, Phys. Rev. B **94**, 075414 (2016).

[24] K. Sasihithlu, J. B. Pendry, and R. V. Craster, Z. Naturforsch. A **72**, 181 (2017).

[25] Z. Q. Zhang, J. T. Lü, and J. S. Wang, Phys. Rev. B **97**, 195450 (2018).

[26] R. Messina, S.-A. Biehs, T. Ziehm, A. Kittel, and P. Ben-Abdallah, arXiv:1810.02628v1.

[27] A. Alkurdi, C. Adessi, S. Li, K. Termentzidis, and S. Merabia, Int. J. Heat Mass Transf. **158**, 119963 (2020).

[28] A. I. Volokitin, JETP Lett. **109**, 749 (2019).

[29] A. I. Volokitin, J. Phys.: Condens. Matter **32**, 215001 (2020).

[30] A. I. Volokitin, Phys. Rev. B **103**, L041403 (2021).

[31] A. Kittel, W. Muller-Hirsch, J. Parisi, S. A. Biehs, D. Reddig, and M. Holthaus, Phys. Rev. Lett. **95**, 224301 (2005).

[32] I. Altfeder, A. A. Voevodin, and A. K. Roy, Phys. Rev. Lett. **105**, 166101 (2010).

[33] K. Kim, B. Song, V. Fernández-Hurtado, W. Lee, W. Jeong, L. Cui, D. Thompson, J. Feist, M. T. Reid, F. J. García-Vidal, et al., Nature **528**, 387 (2015).

[34] K. Kloppstech, N. Könne, S. A. Biehs, A. W. Rodriguez, L. Worbes, D. Hellmann, and

A. Kittel, Nat. Commun. **8**, 14475 (2017).

[35] L. Cui, W. Jeong, V. Fernández-Hurtado, J. Feist, F. J. García-Vidal, J. C. Cuevas, E. Meyhofer, and P. Reddy, Nat. Commun. **8**, 14479 (2017).

[36] A. Jarzembski, T. Tokunaga, J. Crossley, J. Yun, C. Shaskey, R. A. Murdick, I. Park, M. Francoeur, and K. Park, arXiv:1904.09383v2.

[37] B. Derjaguin, Kolloid-Z. **69**, 155 (1934).

[38] P. Yeh, *Optical Waves in Layered Media* (Wiley-VCH, 1988).

[39] P.-O. Chapuis, S. Volz, C. Henkel, K. Joulain, and J.-J. Greffet, Phys. Rev. B **77**, 035431 (2008).

[40] W. Zhang, T. S. Fisher, and N. Mingo, ASME J. Heat Transfer **129**, 483 (2007).

[41] S. Sadasivam, Y. Che, Z. Huang, L. Chen, S. Kumar, and T. S. Fisher, Annu. Rev. Heat Transf. **17**, 89 (2014).

[42] E. Clementi, D. L. Raimondi, and W. P. Reinhardt, J. Chem. Phys. **47**, 1300 (1967).

[43] K. Nakamura, H. Hasegawa, T. Oguchi, K. Sueoka, K. Hayakawa, and K. Mukasa, Phys. Rev. B **56**, 3218 (1997).

[44] C. Caroli, R. Combescot, P. Nozieres, and D. Saint-James, J. Phys. C: Solid State Phys. **4**, 916 (1971).

[45] J. E. Jones, Proc. R. Soc. London, Ser. A **106**, 463 (1924).

[46] C. Li and T. W. Chou, Compos. Sci. Technol. **63**, 1517 (2003).

[47] M. Mohebifar, E. R. Johnson, and C. N. Rowley, J. Chem. Theory Comput. **13**, 6146 (2017).

[48] See Supplemental Material at [URL will be inserted by publisher] for discussions on the short-range [72, 73] and long-range [74] force models, the impact of the electrical double layer effect on the thermal conductance, and the impact of temperature on the heat transfer coefficient.

[49] R. G. Horn and D. T. Smith, Science **256**, 362 (1992).

[50] S. Heinze, X. Nie, S. Blügel, and M. Weinert, Chem. Phys. Lett. **315**, 167 (1999).

[51] N. D. Lang and W. Kohn, Phys. Rev. B **7**, 3541 (1973).

[52] H. Bluhm, A. Wadas, R. Wiesendanger, K.-P. Meyer, and L. Szcześniak, Phys. Rev. B **55**, 4 (1997).

[53] A. Naini and M. Green, Am. J. Phys. **45**, 877 (1977).

[54] S. Srisonphan, M. Kim, and H. K. Kim, Sci. Rep. **4**, 3764 (2014).

[55] J. W. Hong, K. H. Noh, S.-i. Park, S. I. Kwun, and K. Z. G., Phys. Rev. B **58**, 5078 (1998).

[56] S. H. Behrens and G. D. G., J. Chem. Phys. **115**, 6716 (2001).

[57] M. J. Yoo, T. A. Fulton, H. F. Hess, R. L. Willett, L. N. Dunkleberger, R. J. Chichester, L. N. Pfeiffer, and K. W. West, Science **276**, 579 (1997).

[58] H. J. Butt, Biophys. J. **60**, 777 (1991).

[59] D. Anselmetti, T. Richmond, A. Baratoff, G. Borer, M. Dreier, M. Bernasconi, and H. J. Güntherodt, EPL. **25**, 297 (1994).

[60] X. Q. Chen, H. Yamada, H. T., and M. K., J. Vac. Sci. Technol. B **17**, 1930 (1999).

[61] Y. Liu, W. Liu, Z. Wang, W. He, Q. Tang, Y. Xi, X. Wang, H. Guo, and C. Hu, Nat. Commun. **11**, 1599 (2020).

[62] B. D. Terris, J. E. Stern, D. Rugar, and H. J. Mamin, Phys. Rev. Lett. **63**, 2669 (1989).

[63] Y. Martin, D. W. Abraham, and H. K. Wickramasinghe, Appl. Phys. Lett. **52**, 1103 (1988).

[64] D. El Khoury, R. Arinero, J. C. Laurentie, and J. Castellon, AIP Adv. **6**, 035318 (2016).

[65] Y. Hishinuma, T. H. Geballe, B. Y. Moyzhes, and T. W. Kenny, Appl. Phys. Lett. **78**, 2572 (2001).

[66] T. L. Westover and T. S. Fisher, Phys. Rev. B **77**, 115426 (2008).

[67] Y. Wang, T. Liao, Y. Zhang, X. Chen, S. Su, and J. Chen, J. Appl. Phys. **119**, 045106 (2016).

[68] M. V. Berry and K. E. Mount, Rep. Prog. Phys. **35**, 315 (1972).

[69] I. Bâldea and H. Köppel, Phys. Status Solidi B **249**, 1791 (2012).

[70] Y. Zhou, C. Fuentes-hernandez, J. Shim, J. Meyer, A. J. Giordano, H. Li, P. Winget, T. Papadopoulos, H. Cheun, J. Kim, et al., Science **336**, 327 (2012).

[71] L. Olesen, Ph. D., University of Aarhus (1996).

[72] S. Sadewasser and M. C. Lux-Steiner, Phys. Rev. Lett. **91**, 266101 (2003).

[73] N. Yu and A. A. Polycarpou, J. Colloid Interface Sci. **278**, 428 (2004).

[74] S. Belaidi, P. Girard, and G. Leveque, J. Appl. Phys. **81**, 1023 (1997).